LABORATORY EXPERIMENTS ON CURRENT SHEET DISRUPTIONS, DOUBLE LAYERS TURBULENCE AND RECONNECTION

R. L. Stenzel and W. Gekelman
Department of Physics, University of California, Los Angeles, CA 90024

ABSTRACT

The role of laboratory experiments to the understanding of current systems in space plasmas is reviewed. It is shown that laboratory plasmas are uniquely suited to make detailed investigations of basic physical processes in current-carrying plasmas. Examples are given for double layers, current-driven instabilities, and the plasma dynamics at magnetic neutral points during reconnection. Observations of current sheet disruptions show the coupling between local plasma phenomena (double layers) and global circuit properties (magnetic energy storage).

INTRODUCTION

Although laboratory plasmas and astrophysical plasmas consider a vastly different parameter regime, unstable current systems are encountered in both cases. Although the observational methods are opposite, local versus remote, there is evidence for common physical processes: instabilities, plasma energization, reconnection. The investigation of these processes from various viewpoints contributes to the general understanding even though a one-to-one correspondence is often not established.

Carefully designed laboratory experiments establish stable plasmas with simple, known boundary conditions, and a variety of diagnostic tools for in-situ time and space resolved measurements of fields, waves, particle distributions. These features are especially suited for observing localized processes such as double layers which have been well established in the laboratory (Torvén, 1979; Sato, 1982). Similarly, electrostatic and short-scale length electromagnetic turbulence has been successfully studied in many laboratory plasmas carrying currents (Gekelman and Stenzel, 1978; Hollenstein and Guyot, 1983; Stenzel, 1977; Gekelman and Stenzel, 1983). The investigation of magnetic reconnection requires plasmas of larger dimensions, on the order of the ion

M. R. Kundu and G. D. Holman (eds.), Unstable Current Systems and Plasma Instabilities in Astrophysics, 47–60.

collisionless skin depth c/ω_{pi}. In earlier investigations (Baum and Bratenahl, 1980; Frank, 1976; Ohyabu et al., 1974) this has been established by high densities ($n_e \simeq 10^{15}$ cm^{-3}) and small physical sizes (1 ... 10 cm) which makes the diagnostics difficult. Recent reconnection experiments at UCLA (Stenzel and Gekelman, 1979; Gekelman et al., 1982; Stenzel et al., 1983a) have the opposite approach; large scales (1 ... 2m) and medium densities ($n_e = 10^{12}$ cm^{-3}) so as to optimize the diagnostic aspect. In these experiments a classical magnetic neutral sheet has been established; reconnection and particle energization are observed facts. The current sheet associated with the magnetic topology of a flattened X-point exhibits microscopic instabilities (magnetic turbulence) and macroscopic instabilities (current disruptions). The latter case is most interesting since reconnection, current sheet disruptions and double layers occur simultaneously. It is an example of the complicated but probably realistic nonlinear plasma dynamics at magnetic null points which also requires the knowledge of the global circuit properties.

EXPERIMENTAL CONFIGURATION

The UCLA reconnection experiments are performed in a device shown schematically in Fig. 1. A linear discharge plasma column is generated

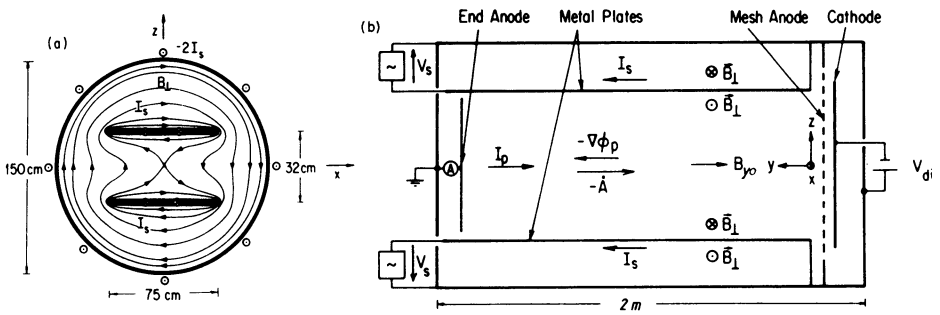

Fig. 1. Schematic picture of the experimental arrangement. (a) Cross-sectional view showing parallel plate electrodes with pulsed currents I_s and magnetic field lines $\vec{B}_\perp$ without plasma. (b) Side view of the device with main electrodes, currents (I_p, I_s) electric fields ($\vec{E} = \dot{\vec{A}} - \nabla\phi_p$), and magnetic fields ($\vec{B} = \vec{B}_\perp + \vec{B}_{yo}$). The coordinate system common in magnetospheric physics has been adopted where y is along the neutral line (device axis), x is along the horizontal neutral sheet, and z is normal to the sheet.

with a 1 m diameter cathode. Detailed plasma diagnostic tools are employed in conjunction with a state-of-the-art digital data processing system. Time and space resolved probe measurements of fields ($\vec{E}$, $\vec{B}$),

https://doi.org/10.1017/S0074180900075501 Published online by Cambridge University Press

plasma properties (n_e, T, ϕ, $\vec{v}$) and distributions [$f(\vec{v}, \vec{r}, t)$] are performed. The analog data are digitized with 100 MHz, 32K A-D converters, evaluated on-line with an array processor linked to a Cray computer.

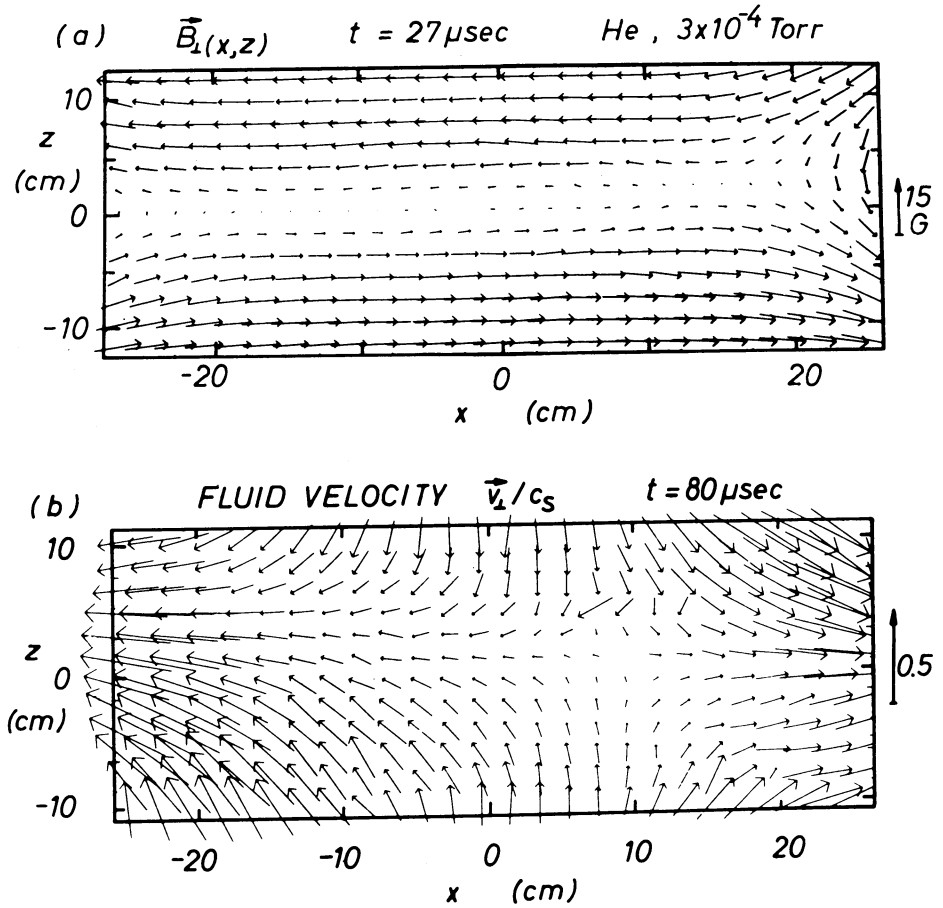

Fig. 2. Measured magnetic fields and flow field during reconnection. (a) Transverse field $\vec{B}_\perp$ (x, z) at a fixed time t, position y = 137 cm, showing the classical neutral sheet topology. (b) Transverse ion flow velocity, $\vec{v}_\perp$ (x, z), normalized to the local sound or Alfvén speed, $c_S = (kT_e/m_i)^{1/2} \simeq c_A = (B^2/2\mu_o nm_i)^{1/2}$. Vertical compression and horizontal jetting are in qualitative agreement with reconnection models.

The plasma of typical density $n_e \simeq 10^{12}$ cm^{-3} and temperature $T_e \simeq 10$ eV is uniform, quiescent, essentially collisionless, and highly reproducible in pulses of duration $t_p \simeq 5$ msec, repeated every $t_r = 2$ sec.

https://doi.org/10.1017/S0074180900075501 Published online by Cambridge University Press

After preparing the plasma in a uniform axial magnetic field ($B_y \simeq 10G$) a pulsed transverse magnetic field ($\langle B_\perp \rangle \simeq 10G$) is applied. Its topology vacuum contains an X-type neutral point along the axis of the device. In the presence of plasma, electron currents are induced which flow preferentially in regions of $B_\perp \simeq 0$. They are so large ($I \simeq 1000A$) as to modify the field topology self-consistently, forming a Dungey (1958) type neutral sheet during the interval of rising applied fields ($0 < t \lesssim 100\mu sec$) shown in Fig. 2a. The corresponding current sheet ($\vec{J} = \nabla \times \vec{B}/\mu_0$) has a thickness ($\Delta z \simeq 5cm$) between the

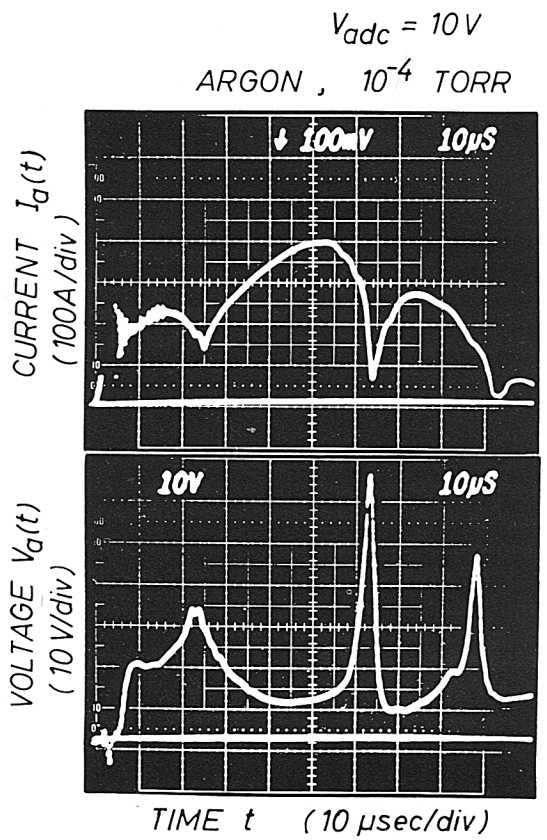

Fig. 3. Disrupted center plate current $I_{a(t)}$ (top trace) and instantaneous plate voltage $V_{a(t)}$ (bottom trace) measured in situ. At each disruption a voltage spike is generated owing to the distributed circuit inductance L. Note that $LdI_a/dt >> V_{adc} = 10V$.

collisionless electron skin depth ($c/\omega_{pe} \simeq 0.6$ cm) and the ion Larmor radius ($r_{ci} \simeq 30$ cm). Thus, we are investigating the fine structure of the diffusion region which is beyond the resolution of present

https://doi.org/10.1017/S0074180900075501 Published online by Cambridge University Press

solar observations and has neither been observed in the magnetosphere. Reconnection occurs in our experiment at a rate indicated by the axial electric field along the separation ($E_y \simeq 0.5$ V/cm) (Sonnerup, 1979) or the normalized inflow velocity of the fluid into the field reversal region ($v/v_A \simeq 0.3$) shown in Fig. 2b (Vasyliunas, 1975). For uniform plasmas and modest current densities (normalized electron drifts $v_d/v_e \simeq 0.1$) the current sheet is macroscopically stable on a time scale long compared with the Alfvén transit time across the sheet.

CURRENT DISRUPTIONS AND DOUBLE LAYERS

The stability of the current sheet with respect to increasing current densities at the separator has been investigated. This is accomplished by raising the potential of the central portion of the end anode on which the plasma terminates axially. When monitoring collected current I_a to this center electrode, we find that at increasing current densities ($v_d/v_e \gtrsim 0.3$) spontaneous current disruptions develop (see Fig. 3a). The cause for this current switch-off has been inferred from detailed diagnostics of the local plasma properties. During a disruption the plasma potential rises in the perturbed current channel to a value much larger than the dc potential ($V_{dc} \simeq 10$V) applied to the end plate (see Fig. 3b). Simultaneously, the plasma density decreases. These processes have a finite axial extent. In particular, the plasma potential exhibits an abrupt axial drop ($\Delta\phi \simeq 30$V in $\Delta y \simeq 5$mm $\simeq 100\lambda_D$), i.e., a double layer is formed in the region where the current is disrupted.

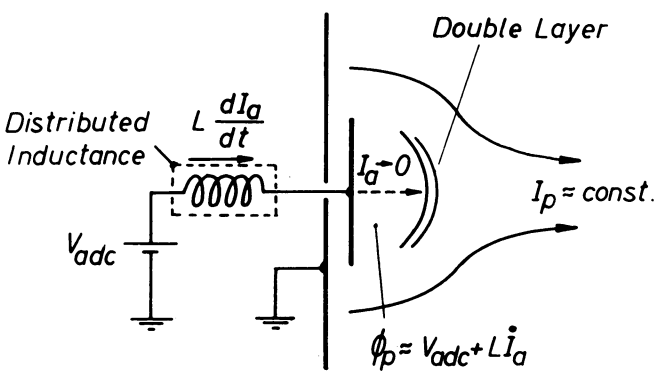

Fig. 4. Schematic diagram of the important elements in the physical model for the disruptive instability

The large positive plasma potential can only be explained in terms of the circuit properties. Fig. 4 shows schematically that the extended current path has a distributed inductance L which, in the presence of a current drop results in an inductive voltage rise LdI/dt.

https://doi.org/10.1017/S0074180900075501 Published online by Cambridge University Press

This voltage drives the plasma potential positive and causes an expulsion of ions, hence a density and current drop. The current decrease in turn reinforces the inductive voltage so that an explosive disruption develops. The current lost in the center of the original sheet is redirected to the sides.

At the double layer particles are accelerated on expense of magnetic field energy stored at different locations in the current system. The kinetic energy first resides in particle beams. Subsequent beam-plasma instabilities transfer the directed energy into waves and heat. For example, microwave emissions at the electron plasma frequency are caused by electron beam-plasma interactions (Whelan and Stenzel, 1981).

Many of the observed phenomena of current sheet disruptions may apply to space plasmas as well. The dynamic current modifications during substorms and solar flares accelerate particles to high energies. The formation of field aligned potential structures is well known from auroral physics but it is possible that nonstationary double layers arise from inductive voltages where the energy storage is remote from the region of dissipation. Type III solar radio bursts involve beam-plasma instabilities possibly analogous to the present emission process.

TURBULENCE IN CURRENT SHEETS

Even in the absence of current disruptions the macroscopically stable neutral sheet exhibits a significant level of turbulence. Currents in collisionless plasmas create various fluid and kinetic instabilities (Das, 1981). The first step in the observation of turbulence is the mode identification from the frequency and wave-number spectrum. Then, the instability mechanism has to be isolated which involves particle distribution measurements. Finally, the effect of the instability on the macroscopic transport properties is of interest. Some of these questions have been addressed in the present experiment.

Three characteristic modes have been identified. An enhanced level of microwave emissions in the range of plasma frequencies ($6 \lesssim f \lesssim 12$ GHz) is observed during reconnection (see Fig. 5 top). These nonthermal emissions are due to electron plasma waves excited by energetic electrons. A second spectrum of waves below the ion plasma frequency has been investigated (Fig. 5 bottom). With two-probe cross-correlation measurements the dispersion $\omega(k)$ is obtained which identifies the noise to consist of ion acoustic modes ($\omega \simeq kc_s$). Finally, low frequency magnetic fluctuations above the lower hybrid frequency ($f_{\ell h} \simeq 200$ kHz) are observed (Fig. 6a) and studied in depth.

https://doi.org/10.1017/S0074180900075501 Published online by Cambridge University Press

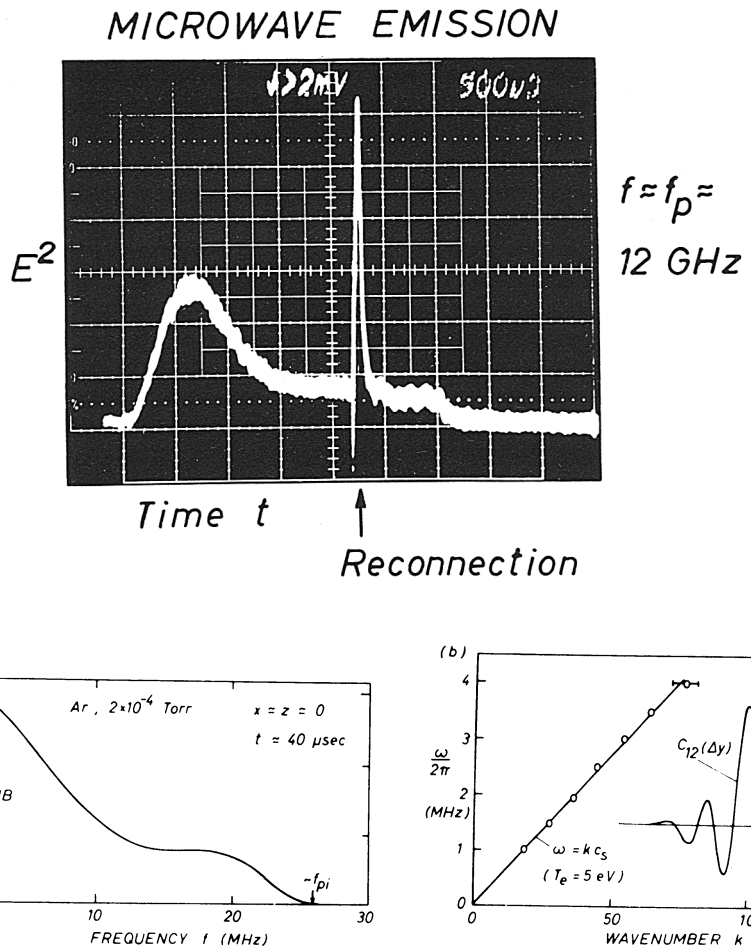

Fig. 5. Turbulence spectra in a current sheet. Top: Microwave emission near the electron plasma frequency is greatly enhanced during the reconnection pulse. Bottom: (a) Electrostatic turbulence spectrum below the ion plasma frequency (~25 MHz) sampled during reconnection. (b) Dispersion relation $\omega(k)$ obtained from measured cross-correlation functions (see insert) identifies spectrum to consist of ion acoustic modes.

The nonstationary magnetic turbulence is analyzed by ensemble averaging two-probe vector cross-correlations. Digital Fourier analysis in time and space reveals a multitude of modes which fall near the average dispersion surface for whistler modes (Fig. 6b). By selecting individual modes the polarization properties $\vec{B}(\Delta\vec{r}, \Delta t)$ are found to be right hand circular, confirming that the modes are indeed whistlers.

https://doi.org/10.1017/S0074180900075501 Published online by Cambridge University Press

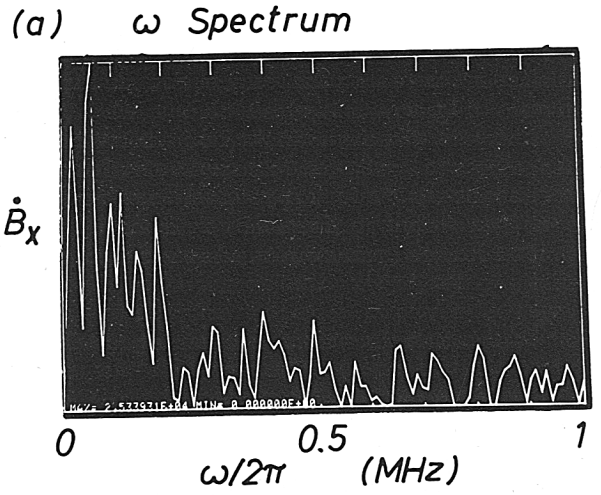

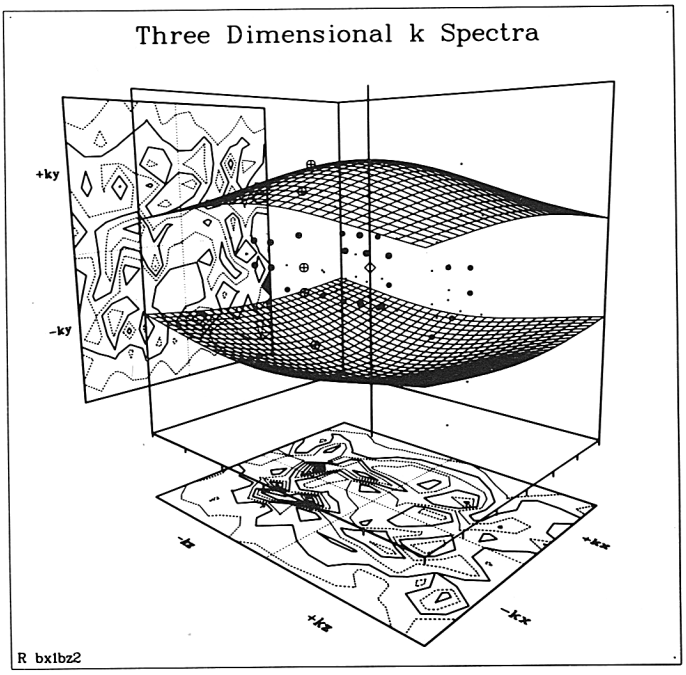

Fig. 6. Magnetic turbulence in a current sheet. (a) Frequency spectrum (lower hybrid $\omega_{\ell h}/2\pi \simeq 0.1$ MHz; electron cyclotron $\omega_{ce}/2\pi \simeq 30$ MHz). (b) Three-dimensional wave vector $\vec{k}$ space with unstable modes of the magnetic turbulence. The cross spectral function $\langle B_{x1}\, B_{z2}\rangle$ at f = 1 MHz has been measured in two orthogonal planes and spatially Fourier transformed. The data points are scattered around the theoretical dispersion surfaces of whistler waves.

https://doi.org/10.1017/S0074180900075501 Published online by Cambridge University Press

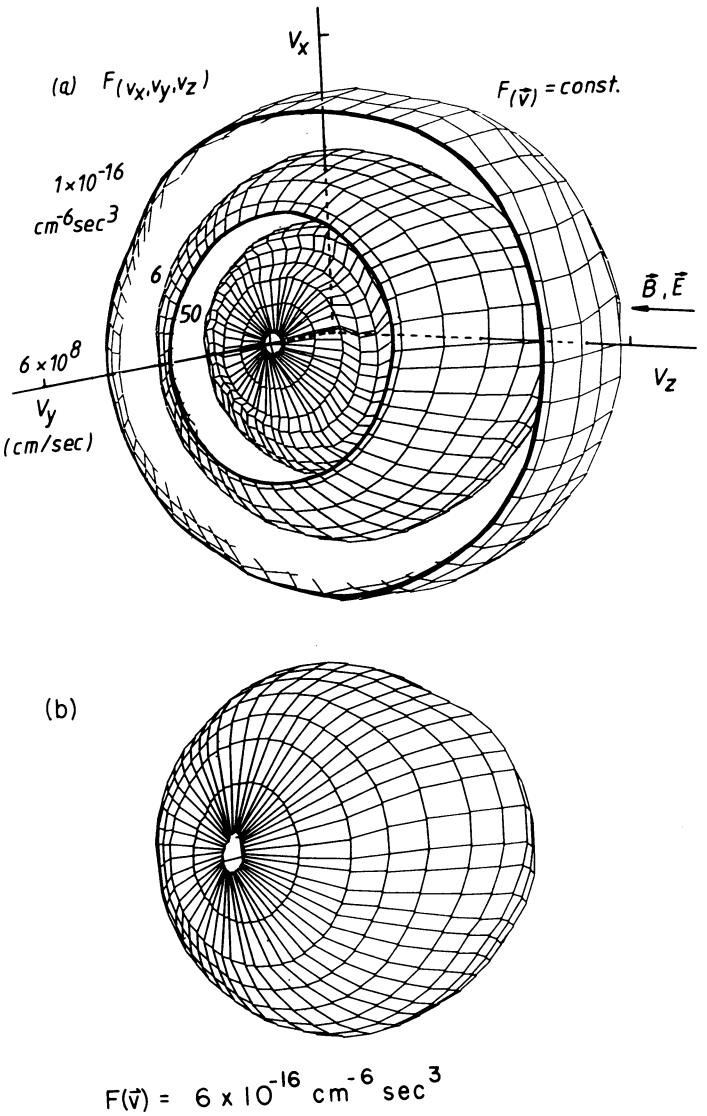

Fig. 7. Display of the distribution function in three-dimensional velocity space as surfaces of constant $f(v_x, v_y, v_z)$. (a) Three nested surfaces cut for purpose of display. Radius expands with decreasing value of $f(\vec{v})$. (b) Complete display of the middle surface showing velocity space anisotropy (nonspherical shape) due to runaway electrons in a current sheet.

https://doi.org/10.1017/S0074180900075501 Published online by Cambridge University Press

Since whistler instabilities can arise from velocity space anisotropies we have investigated the electron velocity distribution function. These measurements are performed with a novel velocity analyzer with good angular resolution ($\Delta\Omega \simeq 10^{-2}$ sterad) (Stenzel et al., 1983b). The three-dimensional distribution $f(v_x, v_y, v_z)$ is displayed in Fig. 7a as surfaces of constant value f, which are nested with the maximum ($f_{max} \simeq 10^{-14}$ cm^{-6} sec^3) near the origin (v = 0). Anisotropies cause deviations from spherical surfaces, clearly visible for the contour f = 6 x 10^{-16} cm^{-6} sec^3 displayed separately in Fig. 7b.

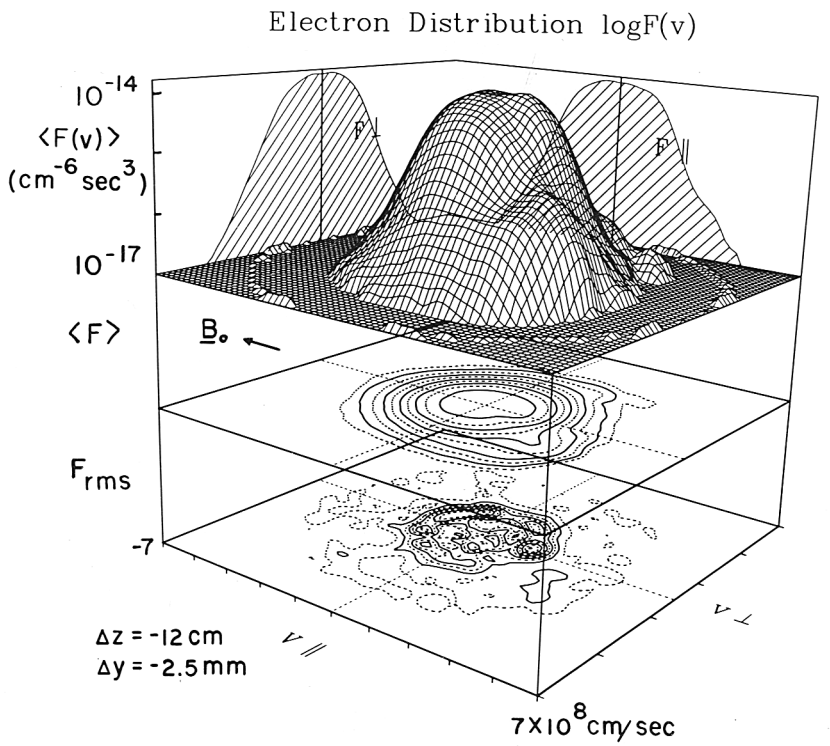

Fig. 8. Comparison of ensemble average distribution $\langle f(\vec{v})\rangle$ and root-mean-square fluctuations $f(\vec{v})_{rms}$. Upper panel shows the mean $\log_{10} \langle f(v_{||}, v_{\perp})\rangle$ and two one-dimensional cuts, $\log_{10} \langle f(v_{||}, 0)\rangle$ and $\log_{10} \langle f(0, v_{\perp})\rangle$. Middle plane shows contours of constant $\langle f(v_{||}, v_{\perp})\rangle$. 3 dB per contour. Lower plane shows fluctuations f_{rms} $(v_{||}, v_{\perp})$, ~4 x 10^{-16}cm^{-6} sec^{+3} per contour. Note anisotropic distribution of fluctuations with approx. maxima where $f(\vec{v})$ exhibits strong gradients.

The elongation along the magnetic field is produced by energetic electrons which runaway in the electric field along the separator. Runaway electrons are observed only inside the neutral sheet. At the sheet edge the normal field component B_z prevents the free acceleration

https://doi.org/10.1017/S0074180900075501 Published online by Cambridge University Press

of electrons.

Kinetic instabilities can be predicted both from the shape of the average distribution function (e.g. $\partial f/\partial \vec{v} > 0$) and by fluctuations in the distribution involving wave-particle resonances. From a large ensemble of repeated measurements we have determined both the mean value and the rms fluctuations which are displayed in Fig. 8 in a two-dimensional velocity space. Comparing the contour plots of f_{mean} ($v_{||}$, $v_{\perp}$) and f_{rms} ($v_{||}$, $v_{\perp}$) we find enhanced fluctuations near the anisotropic runaway electrons. The particle velocities correspond to the Doppler shifted phase velocities of unstable whistlers, and their fluctuation spectra overlap. Thus, the origin of the whistler wave turbulence appears to lie in the observed nonequilibrium distributions in the current sheet.

The complete knowledge of the distribution function $f(\vec{v}, \vec{r}, t)$ provides us with the space-time resolved fluid properties of which we have calculated the particle density, current density, mean energy and heat flow. Transport parameters have been studied with the help of an array probe which provides the bulk electron temperature with high time resolution (Wild, et al., 1983). Correlation analysis of temperature fluctuations in the current sheet indicate that heating occurs in bursts of short durations ($\Delta t \simeq 3\mu$sec) generated in narrow regions ($\lesssim$ 3 cm diam.) propagating and diffusing across the field at approximately the Alfvén speed. Heat bursts correlate with current pulses. The cross-field heat conductivity is larger than the classical value. The microscopic heating and transport processes in collisionless plasmas undoubtedly involve plasma turbulence effects, but further investigations are required to understand the processes in detail. Laboratory plasmas are highly suited for this task.

ACKNOWLEDGMENTS

The authors acknowledge helpful assistance in this work from N. Wild and J. M. Urrutia. This research was sponsored in part by the National Science Foundation (ATM 81-19717, PHY 82-09524), the National Space and Aeronautics Administration (NAGW-180) and the Air Force Office of Scientific Research (F19628-82-K0019).

REFERENCES

Baum, P. J. and Bratenahl, A.: 1980, in C. Marton (ed.), *Advances in Electrons and Electron Physics*, Academic, New York, Vol. 54, p. 1.
Das, A. C.: 1981, in H. Kikuchi (ed.), *Relation Between Laboratory and Space Plasmas*, D. Reidel Publ. Co., Dordrecht, Holland, p. 241.
Dungey, J. W.: 1958, *Cosmic Electrodynamics*, Cambridge University Press, New York.
Frank, A. G.: 1976, *Proc. P. N. Lebedev Phys. Inst. Acad. Sci. USSR Engl. Transl.*, 74, 107.

https://doi.org/10.1017/S0074180900075501 Published online by Cambridge University Press

Gekelman, W. and Stenzel, R. L.: 1978, *Phys. Fluids* 21, 2014.
Gekelman, W., Stenzel, R. L., and Wild, N.: 1982, *Physica Scripta* T2/2, 277.
Gekelman, W. and Stenzel, R. L.: 1983, *J. Geophys. Res.* (submitted).
Hollenstein, Ch. and Guyot, M.: 1983, *Phys. Fluids* 26, 1606.
Ohyabu, N., Okamura, S., and Kawashima, N.: 1974, *J. Geophys. Res.* 79, 1977.
Sato, N.: 1982, in P. Michelsen and J. J. Rasmussen (eds.), *Symposium on Plasma Double Layers, Risø National Laboratory, June 16-18, 1982*, Risø-R-472, p. 116.
Sonnerup, B. U. O.: 1979, in *Space Plasma Physics: The Study of the Solar System*, National Academy of Sciences, Washington D. C., Vol. 2, p. 879.
Stenzel, R. L.: 1977, *J. Geophys. Res.* 82, 4805.
Stenzel, R. L. and Gekelman, W.: 1979, *Phys. Rev. Lett.* 42, 1055.
Stenzel, R. L., Gekelman, W., and Wild, N.: 1983a, *J. Geophys. Res.* 88, 4393.
Stenzel, R. L., Gekelman, W., Wild, N., Urrutia, J. M., and Whelan, D.: 1983b, *Rev. Sci. Instrum.* 54 (in press).
Torvén, S.: 1979, in P. J. Palmadesso and K. Papadopoulos (eds.), *Wave Instabilities in Space Plasmas*, D. Reidel, Hingham, Mass., p. 109.
Vasyliunas, V. M.: 1975. *Rev. Geophys. Space Phys.* 13, 303.
Whelan, D. A. and Stenzel, R. L.: 1981, *Phys. Rev. Lett.* 47, 95.
Wild, N., Stenzel, R. L., and Gekelman, W.: 1983, *Rev. Sci. Instrum.* 54, (in press).

DISCUSSION

Sonnerup: What is the ion gyroradius? What is the reconnection rate?

Stenzel: The calculated ion Larmor radius is $r_{ci} \simeq 30$ cm for Argon, $r_{ci} \simeq 10$ cm for Helium at $\langle B \rangle \simeq 20$ G. The reconnection rate, as determined by the observed upstream inflow velocity, is given by

$$M = \frac{v}{v_A} \simeq 0.2.$$

Van Hoven: What is the driving electric field strength ($E/E_{Dreicer}$) when you show disruptions? Is there any E-field threshold for this behavior?

Stenzel: We are in the regime where the electron drift velocity approaches the thermal velocity or $E/E_{Dreicer} \simeq 1$. There are no disruptions observed for $v_d/v_e \simeq 0.1$; they build up in the range $0.2 \lesssim v_d/v_e \lesssim 1$.

Benford: Your 6 GHz radiation seems to be evidence for strong electromagnetic emission near ω_p. What is the efficiency of this radiation, and how does it compare, roughly, to microwave emission from flaring loops and type III bursts?

Stenzel: Microwave signals at $f \simeq f_p \simeq 6$ GHz are observed both as electrostatic signals in the beam-plasma region and as electromagnetic

https://doi.org/10.1017/S0074180900075501 Published online by Cambridge University Press

waves outside the plasma. The mode conversion on density gradients and scattering off ion acoustic modes has a rather low efficiency, estimated to be $P_{em}/P_{es} \simeq 10^{-4}$. I have pointed out the qualitative analogy between type III solar radio bursts and our ω_p emission which occur during impulsive reconnection events.

Sato: Can you distinguish between double-layer acceleration and the acceleration by reconnection (slow shocks, for example)?

Stenzel: Yes, the acceleration by the double layer is mainly in the direction of the separator (y-axis) while the acceleration due to the reconnection is in the direction of the neutral sheet (x-axis).

Kundu: With regard to 6 GHz plasma emission, I believe that the time structure of these microwave bursts is less than 10 μs. Does it mean that in an astrophysical object such as the solar flare plasma, one should be able to produce such fine time structure bursts intrinsically, except for the fact that other effects may modify such time structures?

Stenzel: The time scale for the current distruption and associated microwave bursts is roughly given by the ion transit time through the perturbed current channel, here $\tau \simeq 5$ cm/$(5\times10^5$ cm/sec$) \simeq 10$ μsec. If a solar flare of similar plasma parameters would exhibit a multitude of unstable current filaments of comparable scale size one may indeed expect the emission to be randomly modulated at the above mentioned time scale.

Birn: In magnetotail simulations the asymmetry of the configuration with gradients parallel to the current sheet and a magnetic field component perpendicular to it seems to have an important effect. Could you study such effects with your device?

Stenzel: Yes, such studies could be done. We could establish such asymmetries by inclining the current-carrying plates at an angle with respect to one another.

Dum: You pointed out the importance of the electrodynamics of the plasma and external circuit for Double Layer (DL) formation. I think this is a very significant point for our going beyond the usual electrostatic laminar solution of the one dimensional Vlasov equation that is offered as an explanation even for such highly dynamic processes as auroras. Nevertheless, particles are also important. What do you think are the particle boundary conditions essential to DL formation such as injection or reflection from electrodes, etc. In the very recent experiment of Guyot and Hollenstein (Phys. Fluids 1983) DL formation seems to depend on whether one electrode is heated or not. How do you trigger DL in a controlled manner, as you mentioned?

Stenzel: The anode, which is the only relevant boundary, absorbs all electrons; thus we have no control over the injected particle distributions as in Hollensteins work.

I mentioned that we now trigger current disruptions (not necessarily double layers) in a controlled manner. This is done by pulsing a thin slab of magnetic field (B_z) transverse to the current sheet (J_y) which causes a total current disruption. Large inductive voltages drop off across the slab, possibly forming again double layers.

Bratenahl: Did I understand that you are now looking for spontaneous development of double layers; that is, double layer development without artificial stimulation?

https://doi.org/10.1017/S0074180900075501 Published online by Cambridge University Press

Stenzel: The work reported did describe spontaneous development of double layers without artificial stimulations. We are now working on controlled disruptions of the entire current sheet.

D. Smith: You mention that when a double layer forms, a 3-D potential results with radial ion acceleration. Could you explain in more detail how this occurs?

Stenzel: The potential structure is three-dimensional, since only the perturbed central part of the current sheet rises to a large positive potential over a finite axial length. Since the ions are unmagnetized, they are accelerated in both radial and axial directions. This leads to a large ion, hence density loss from the perturbed current channel. The pump-out of plasma ultimately causes the current loss.

Henriksen: Does the electron distribution have a characteristic shape in velocity space?

Stenzel: Yes, we have made extensive measurements of the electron distribution function and found asymmetric distributions even without current dusruptions. The current sheet contains a large number ($\sim$ 10%) of runaway electrons which are accelerated by the inductive electric field along the separator. These particles strongly influence the transport processes and provide a source of free energy for driving various microinstabilities.

https://doi.org/10.1017/S0074180900075501 Published online by Cambridge University Press